UCRL-JRNL-229819

LAWRENCE
LIVERMORE
NATIONAL
LABORATORY

The importance of EBIT data for Z-pinch plasma diagnostics

A. S. Safronova, V. L. Kantsyrev, P. Neill, U. I. Safronova, D. A. Fedin, N. D. Ouart, M. F. Yilmaz, G. Osborne, I. Shrestha, K. Williamson, T. Hoppe, C. Harris, P. Beiersdorfer, S. Hansen

April 10, 2007

Canadian Journal of Physics

Disclaimer

The importance of EBIT data for Z-pinch plasma diagnostics

A. S. Safronova [1*], V. L. Kantsyrev [1], P. Neill [1], U.I. Safronova [1], D.A. Fedin [1], N.D. Ouart[1], M.F. Yilmaz[1], G. Osborne [1], I. Shrestha[1], K. Williamson[1], T. Hoppe [1,2], C. Harris[3], P. Beiersdorfer[4], S. Hansen[4]

[1]Physics Department, MS 220, University of Nevada, Reno, NV 89557

[2]Drexel University, PA 19104

[3]Gulf Coast Community College, Panama City, FL 32401

[4]Lawrence Livermore National Laboratory, Livermore, CA 94550

PACS: 32.30.Rj, 52.58.Lq, 52.70.La

*Corresponding author e-mail: alla@physics.unr.edu

Abstract

The results from the last six years of x-ray spectroscopy and spectropolarimetry of high energy density Z-pinch plasmas complemented by experiments with the electron beam ion trap (EBIT) at the Lawrence Livermore National Laboratory (LLNL) are presented. The two topics discussed are the development of M-shell x-ray W spectroscopic diagnostics and K-shell Ti spectropolarimetry of Z-pinch plasmas. The main focus is on radiation from a specific load configuration called an "X-pinch". X-pinches are excellent sources for testing new spectral diagnostics and for atomic modelling because of the high density and temperature of the pinch plasmas, which scale from a few μm to several mm in size. They offer a variety of load configurations, which differ in wire connections, number of wires, and wire materials. In this work the study of X-pinches with tungsten wires combined with wires from other, lower-Z materials is reported. Utilizing data produced with the LLNL EBIT at different energies of the electron beam the theoretical prediction of line positions and intensity of M-shell W spectra were tested and calibrated. Polarization-sensitive X-pinch experiments at the University of Nevada, Reno (UNR) provide experimental evidence for the existence of strong electron beams in Ti and Mo X-pinch plasmas and motivate the development of x-ray spectropolarimetry of Z-pinch plasmas. This diagnostic is based on the measurement of spectra recorded simultaneously by two spectrometers with different sensitivity to the linear polarization of the observed lines and compared with theoretical models of polarization-dependent spectra. Polarization-dependent K-shell spectra from Ti X-pinches are presented and compared with model calculations and with spectra generated by a quasi-Maxwellian electron beam at the LLNL EBIT-II electron beam ion trap.

1. Introduction

The first x-ray spectra of M-shell W were produced by high-density exploded–wire plasmas more than 25 years ago [1]. The precision of the measurements of Ni-like W lines was improved in laser plasma experiments [2]. The extended analysis of Ni-like W spectra from laser plasma has included $nf \to 3d$ (n=5-9), $nd \to 3p$ (n=4-6), and $np \to 3s$ (n=4,5) transitions [3]. Tungsten wire arrays were studied extensively on the Z accelerator at Sandia National Laboratories (SNL) since 1998 when it was shown that they can produce x-ray powers up to 200 TW and x-ray energies up to 2 MJ [4-5]. Since then, despite an increasing number of papers about the implosions of W arrays on the SNL-Z machine and their recent applications to inertial confinement fusion [6-7], x-ray M-shell diagnostics of tungsten HED plasmas have not yet been developed.

In this paper we present a theoretical model of M-shell W spectra. This model was benchmarked with LLNL EBIT data produced at different energies of the electron beam and recorded by crystal spectrometers and a broadband microcalorimeter. Moreover, high temperature and density plasmas were produced from the variety X-pinches on 1 MA Zebra device at UNR. In particular, M-shell W radiation was generated by the implosions of X-pinches with tungsten wires combined with the wires from other lower-Z wire material such as Al and Mo. These data are also presented.

An X-pinch plasma is formed by touch-crossing two wires between the electrodes of a high-current pulsed power generator. The current quickly vaporizes and strongly ionizes the wire material. As a result, an X-pinch yields short x-ray bursts from one or more small bright spots at the intersection of the crossed wires. X-pinches are a good source for studying the dynamics of Z-pinch plasmas of very small sizes, high densities, and temperatures for developing 1-10keV x-ray backlighters.

Currently, x-ray spectra of X-pinches are collected and studied at different pulsed power machines, for example, at the university-scale 1 MA Zebra device at University of Nevada, Reno [8-12] and Cobra facility at Cornell University (CU) [11-12], as well as at smaller devices such as at a 450 kA pulsed power device at CU [13]. It was shown that X-pinch plasma can reach temperatures of 2-3 keV and densities up to 10^{23} cm^{-3}. Another distinct feature of X-pinches is the existence of plasma anisotropy in the form of strong electron beams, which makes them attractive objects for spectropolarimetry (a powerful tool for studying the anisotropy of high temperature plasmas).

Because of the high temperature and density polarized emission from X-pinch plasma is complicated and we first investigated the polarization properties of K-shell Ti lines using the LLNL EBIT. EBIT is very important for the study of polarization because it is capable of producing x-ray lines by the beam of non-Maxwellian electrons at well-controlled experimental conditions, which includes, for example, selection of the atomic process, ionization stage, and value of the electron beam. Our previous work on x-ray line polarization at LLNL EBIT included the study of polarization-dependent spectra of x-ray dielectronic satellites of Li- and Be-like [14-15] and B-like Fe ions [16]. In the present paper we analyze polarization-dependent Ti K-shell spectra generated by a quasi-Maxwellian electron beam at the LLNL EBIT and compare this analysis with K-shell spectra from Ti X-pinches obtained at UNR.

2. M-shell W radiation from LLNL EBIT and UNR X-pinch experiments

2.1. M-shell W model: atomic and plasma physics in the model

Our non-LTE collisional radiative (CR) model of the M-shell W emission has about 4000 levels, and includes the ground states from all ions from neutral to bare W and a detailed structure for Cr- to Se-like W ions [11]. Energy level structure and complete radiative coupling as well as a subset of collisional data were calculated using the FAC code developed by M. F. Gu [17]. For complete collisional coupling among excited levels, the Van Regemorter approximation was used, which can lead to some overestimation in the electron temperature.

The energies for the excited states for the transitions 3l-4l’, 3l-5l’’, and 3l-6l’’’ as well as radiative transition probabilities in Ni-like W were also determined to second order in Relativistic Many Body Perturbation Theory (RMBPT) [18-20]. The calculations start from a closed-shell Dirac-Fock potential, and include second-order Coulomb and Breit-Coulomb interactions. Electric-dipole matrix elements are calculated in second order for transitions from excited states to the ground state. Table 1 lists the atomic data calculated for the most intense lines in Ni-like W specified in LS coupling. In particular, the spectral lines N1-N10 are allowed electric-dipole (E1) transitions, i.e. transitions of the type 3-6 (N1, N2), 3-5 (N3 and N4), and 3-4 (N5-N10). The spectral lines N11 and N12 are forbidden 3-4 electric-quadrupole (E2) transitions. The comparison of RMBPT and FAC atomic data calculated for the observable transitions in Ni-like W in Table 1 shows a good agreement.

2.2. Modeling of the M-shell W spectra from the LLNL EBIT

M-shell W spectra produced at the LLNL EBIT-I and EBIT-II electron beam ion traps were collected in two different experiments using a crystal spectrometer and an engineering model of the x-ray spectrometer (XRS) microcalorimeter from the Suzaku x-ray satellite mission. In the experiments with a crystal spectrometer on EBIT-II, the M-shell W spectra were produced at eleven different values of the electron beam E_b ranging from 2.4 keV to 4.6 keV. This spectrometer covered the spectral region from 5 to 6 Å with a spectral resolution of 2200. The analysis of these spectra was given in [21]. Here we show some of these spectra and make a comparison with our new non-LTE models. In particular, the experimental M-shell W spectra recorded with the crystal spectrometer and produced at E_b=3.6, 3.9, and 4.3 keV are presented along with our modeling results in Figs. 1, 2, and 3, respectively. The Ni-like W lines N6, N7, and N5 dominate the spectra produced at E_b=3.6 and 3.9 keV (see Figs. 1 and 2), and the Cu-like lines Cu1 and Cu2 are much less intense than the Ni-like lines. Moreover, the two M-shell W spectra are almost the same for these two electron beam energies. By contrast, the spectrum at E_b=4.3 keV is different (see Fig. 3). Though the same three Ni-like lines are still intense, spectral lines from higher ionization stages (Co1, Co2, and Fe1) appear because this electron beam energy exceeds the ionization potential of Ni- and Co-like W. In general, modeling (top) reproduces well the experimental spectra (bottom) in all three figures as discussed early in [22].

The XRS microcalorimeter as fielded on EBIT-I was capable of acquiring, filtering, and characterizing x-ray events on 32 independent pixels as described in [23-24]. This spectrometer calorimeter recorded the spectra in a broader spectral range (from 3 to 8 Å) and with about 6 times less resolution than the crystal spectrometer. In these experiments only 14 pixels were used, and each pixel functioned simply as one of 14 independent spectrometers. The fourteen M-shell spectra produced at E_b=3.9 keV and recorded by the XRS in experiments on EBIT-I are presented in Fig. 4. This figure demonstrates the good reproducibility of this device. In Fig. 5 the experimental spectrum (bottom) from one of the spectra shown in Fig. 4 is presented along with the modeling (top). This spectrum is similar to the one recorded by the crystal spectrometer in Fig. 2 but covers a broader spectral range from 3 to 9 Å. As a result, it includes not only the three lines Ni6, Ni7, and Ni5 but also the other Ni-like lines from Table 1. The theoretical synthetic spectrum at the top of Fig. 5 is calculated using the non-LTE kinetic model of W with a Gaussian electron distribution function of 50 eV full width half maximum (FWHM) centered at E_b=3.9 keV. This is the same as the one used for the synthetic spectrum in Fig. 2. All twelve lines Ni1-Ni12 are reproduced well by our theory.

2.3. Comparison of the M-shell W spectra from the LLNL EBIT and UNR X-pinches and modeling of the UNR X-pinch experiments

X-pinches with tungsten wires combined with wires from other, lower-Z wire material such as Al and Mo were used in experiments on the 1MA pulsed power generator Zebra at UNR to produce and study M-shell radiation from W ions. We have found that using combined X-pinches consisting of one or a few W wires and the rest of the wires from a lower-Z material (such as Mo or Al) provides better quality M-shell W spectra than when using only W wires [11-12]. The experimental Al/W X-pinch spectrum is shown at the top of Fig. 6. It was a planar-loop X-pinch with a 99 μm Al 5056 wire in the anode loop and a 35 μm W wire in the cathode loop. The experimental spectrum includes both K-shell radiation from Al and Mg (Al 5056 has 95% Al and 5% Mg) and M-shell radiation from W. The line designation for all K-shell lines (Al, Mg, and Ti) is the same throughout the paper. For example, Al1 is the He_{α} line, Al2 is the Ly_{α} line, and Al3 is the He_{β} line of Al for K-shell Al.

EBIT spectra were very useful in the identification of M-shell W spectra from the implosion of combined X-pinches. The comparison of the Al/W X-pinch spectrum (Fig. 6, top) with the experimental LLNL EBIT spectrum (Fig. 5 and Fig. 6, bottom) reveals the 3-4 transitions (N5-N10) and 3-5 transitions (N3 and N4) in Ni-like W.

The experimental W/Mo X-pinch spectrum is shown at the top of Fig. 7. It was a planar-loop X-pinch with a 35 μm W wire in the anode loop and a 50 μm Mo wire in the cathode loop. The experimental spectrum includes both L-shell radiation from Mo and M-shell radiation from W. The comparison of the W/Mo X-pinch spectrum (Fig. 7, top) with the experimental LLNL EBIT spectrum (Figs. 5, 6, 7, bottom) reveals the 3-4 transitions (N5-N10). Because 3-5 transitions in Ni-like W overlap with 2-3 transitions in L-shell Mo, the lines N3 and N4 could not be assigned to particular peaks in this X-pinch spectrum. Figure 8 shows the M-shell W modeling of the above mentioned combined X-pinch spectra at an electron temperature Te=1 keV, electron density Ne=10^{21} cm^{-3}, and a small portion of non-Maxwellian electrons f=0.03 (for more about the influence of hot electrons on x-ray spectra, see, for example, [25-26]). Modeling describes well the most intense peaks and the ratio between 3-5 and 3-4 transitions in Ni-like W. However, more work is needed to match the intensities of higher and lower ionization stages. It is important to note that forbidden E2 transitions Ni11 and Ni12, which are present in spectra from low-density sources, are not observed in the X-pinch spectra.

3. K-shell Ti radiation from the LLNL EBIT and UNR X-pinch experiments

K-shell Ti lines important for diagnosing low-density plasmas are listed in Table 2. They include the He-like lines, in particular the He α resonance line (w), the intercombination line IC (y), the forbidden lines x and z, and the inner-shell satellite lines of Li-like ions q and r. All these lines are often used in the diagnostics of Ti plasmas from tokamaks [27, 28] and electron beam ion traps [29]. In addition to these lines, the He-like resonance line Heβ, the H-like resonance line Lyα, the satellite line of Be-like ions (Be) and the "cold" K α lines of Ti are used in the diagnostics of X-pinch plasmas. The data from two polarization-sensitive experiments at the LLNL EBIT will be considered. The first experiment involved the measurement of x-ray line polarization of K-shell Ti lines excited by a monoenergetic beam [30]. The polarization-sensitive x-ray spectrum of He-like Ti was produced at the energy just above the electron-impact excitation threshold, 4800 eV (and thus below the KMM dielectronic resonances). The measured intensities were simultaneously recorded by spectrometers with a Si (220) crystal, which records an almost pure parallel polarization state, and with a Si (110) crystal, which records a mixture of both polarization states [30]. In the second experiment the same technique was used, but the K-shell Ti spectra were generated by a quasi-Maxwellian electron beam [31]. The details of the technique for producing a quasi-Maxwellian electron beam and its implementation at the LLNL EBIT facility can be found in [32, 33]. In the second experiment [31] the measured intensities were simultaneously recorded by spectrometers with a Si (220) crystal (observing an almost pure parallel polarization state) and with a Ge (111) crystal (observing a mixture of both polarization states). The ratios of the relative intensities of K-shell Ti lines from these two LLNL EBIT experiments are listed in Table 3.

3.1. Modeling of x-ray K-shell Ti spectra

In this section we focus on the data from the two spectrometers employing Si (111) and Ge (111) crystals, which are the least sensitive to polarization, i.e. on the ratios I_2 and I_4, respectively (see Table 3). The non-LTE CR Ti model was applied to analyze these data (for the details of the model, see [25-26]). In Fig. 9 theoretical synthetic spectra of K-shell Ti are shown calculated at low density for two different electron distribution functions (EDF): a Gaussian centered at 4.8 keV (gray line) and a Maxwellian at T_M=2.3 keV (black line). Theory describes well the ratios and differences in spectra between monoenergetic (Gaussian) and quasi-Maxwellian beams. For example, the ratios x/w and y/w are more than 50% larger for the Gaussian EDF (I_2) than for the Maxwellian EDF (I_4) while the ratio z/w is almost unchanged. However, the modeling does not show any line q (Li-like inner-shell satellite at 2.6277 Å) for the Gaussian EDF. It is suppose to be about 30% of the w line according to the experimental ratios in Table 3. This problem is likely related to the fact that the charge balance in EBIT was shifted toward lower charge states in this measurements, and is not a polarization effect.

Now we will consider the K-shell Ti spectra produced by the 1MA pulsed power Zebra generator at UNR. A typical Ti X-pinch spectrum as well as our modeling results using the non-LTE CR Ti model mentioned above is shown in Fig. 10. The modeling of the Ti X-pinch spectrum indicates that the emission comes from at least two different regions: a hot dense region and a cooler and probably less dense region. In particular, the synthetic spectrum at the top (Fig. 10a) is calculated at Te=1 keV and Ne =10^{21} cm^{-3} and represents the region of Ti plasma with intense He-like lines Ti1 (w, He α), Ti1'(y), Ti3 (Heβ) and the Li-like satellites Ti3'. The synthetic spectrum in the middle (Fig. 10b) is calculated at Te=2.2 keV and Ne=10^{22} cm^{-3} and represents the hot and dense region with intense H-like line Ti2 (Ly α) as well as intense He-like lines Ti1 (w, He α) and Ti3 (He). In addition to these two plasma regions, there may be the third region, which is even cooler than the first one. It emits radiation from Li-like, Be-like, and other lower-ionization ions. These satellites are located on the right from the line y at λ>2.625 Å. The "cold" Ti K α line (Ti4) indicates the presence of very low temperature plasma (<20 eV) and is not modeled here. The detailed temperature determination using "cold" Ti K α line from laser-plasma interaction experiments is presented in [34].

3.2. **Polarization of x-ray line radiation: calculations and applications to the experiments**

Ti X-pinch experiments on the 1 MA Zebra at UNR provided experimental evidence of the existence of strong electron beams. This motivated the development of a new diagnostics, x-ray spectropolarimetry, for investigating the anisotropy of the plasma EDF. X-ray spectropolarimetry is based on the knowledge of the polarization properties of radiation. An excellent test bed for the study of x-ray line polarization and the benchmarking of the polarization-sensitive calculations (as was mentioned in Introduction) is EBIT.

We begin with a calculation of the polarization of lines that will be applied to experiments at the LLNL EBIT and then to X-pinch experiments on Zebra at UNR. Values of the polarization of the most diagnostically important lines were calculated using the FAC code [17] and are presented in Fig. 11 and in Table 4. The lines listed in Table 2 are produced by the electron impact excitation, and thus their polarization is shown as a function of electron beam energy. The polarization of the most intense line w has its maximum (~60%) near the excitation threshold (~4.7. keV) and then gradually decreases towards zero and is less then 10% at ten times threshold. By contrast, the polarization of line y changes non-monotonically with the energy of the electron beam. It is negative near threshold (~-30%), then changes sign and becomes ~+30% already at 3 times threshold. Then it approaches the polarization of the w line. Hence, when the measured polarization of the w and y lines is the same then the energy of electron beam is higher than 30 keV and when it is different then it indicates a low-energy electron beam with the energy close to the threshold or only somewhat higher. This result is important in diagnosing the energy of beams in plasmas.

In Table 4 the degree of polarization for the K-shell Ti lines excited by a monoenergetic electron beam with energy of 4.8 and 11.5 keV is given. In particular, the measured values of polarization obtained using the measured intensities (see Table 3) and a two-crystal technique from [30, 35] along with theoretical predictions from [30] are listed for E_b=4.8 keV. The ratio of intensities I_1/I_2 from Table 3 close to 1 indicates almost equal values of polarization of two lines. For example, this ratio I_1/I_2=0.99 for q/w (see Table 3) and corresponding degrees of polarization for lines w and q are both ~ 0.4 (see Table 4). The ratio of intensities I_1/I_2 = 0.75 for z/w and the corresponding degree of polarization of the line z is -0.101. The smallest ratio of I_1/I_2 = 0.53 for x/w results in the most negative value of polarization of this line (-0.48). Our theoretical values of x-ray line polarization calculated at 4.8 keV agree well with the measured values and the theoretical values from [30].

The theoretical values of polarization calculated at E_b=4.8 keV and 11.5 keV show limits within which the polarization is changing in the experiment with a quasi-Maxwellian electron beam (the second experiment discussed in the beginning of this section). As was discussed before polarization of the line y changes the most (from -

0.308 to +0.228), which may result in almost zero polarization. Polarization of other lines only slightly changes, in particular decreases for positively polarized lines (w and q) and increases for the negatively polarized lines (z and x). To employ the two-crystal technique we need to make an assumption about the value of polarization of the certain line. If we assume the polarization of the line w is 0.5 then using the polarization-sensitive ratios I_3/I_4 for the lines y, z, and x we estimate polarization of almost zero for the line y (I_3/I_4 =0.74), ~-0.2 for the line z (I_3/I_4 =0.63), and ~-0.48 for the line x (I_3/I_4 =0.47). These values of polarization fall within the corresponding limits from Table 4. They also correlate well with the above analysis of the intensity ratios I_1/I_2 from Table 3. On the contrast, the estimate for polarization of the line q gives a small negative value, which does not agree with our prediction (see Table 4). This will be a subject of future work.

In a Maxwellian plasma dielectronic satellite transitions play an important role and several n=2 satellites produced by the processes $1s^2 + e^- \rightarrow 1s2l2l'$ and $1s^22s + e^- \rightarrow 1s2s2l2l'$ are seen. This is illustrated in Fig. 12 where we show the dielectronic satellite spectra of Li-like (lines j, k, s, m, and t) and Be-like Ti recorded by the Si (220) crystal in the experiment with a quasi-Maxwellian electron beam from [36]. The theoretical polarizations-sensitive spectra describe the experiment well. The details of calculations of atomic and polarization characteristics of these transitions in Ti ions are given in [37].

The K-shell line radiation from Ti X-pinches was recorded by a polarimeter, which includes so-called horizontal (H) and vertical (V) spectrometers. The experimental details including the diagnostic setup were described in [38-39]. Briefly, the "H "spectrometer has a dispersion plane perpendicular to the discharge axis and records mostly the parallel polarization state. The "V" spectrometer has a dispersion plane parallel to the discharge axis and records mostly the perpendicular polarization state. Both "H " and "V" spectrometers were two identical convex crystal spectrometers utilizing LiF crystals with a lattice spacing (2d=4.027Å) corresponding to nominal Bragg angles from 40.6° (for Ti1 line) up to 42.9 ° (for Ti4 line). Typical spectra recorded by the "H" and "V" spectrometers are presented in Fig. 13 (shot 39). The experimental intensity ratios of the K-shell Ti lines with the wavelengths providing the Bragg angle closest to 45° (Ti1, Ti1', Ti1'', Ti1''', and Ti4) are listed in Table 5 for three selected shots where Ti X-pinches were made from 30μm Ti wires. The experimental intensities ratios in Table 5 are associated with different polarization states $I_{II}/I_{\perp}$ for each of the spectral lines from the horizontal and vertical spectra (H/V). A ratio $I_{II}/I_{\perp}$ greater (less) than unity for a given line indicates positive (negative) polarization of the line. We believe that line polarization occurred in shot 39, where the largest deviations from unity have been observed. For this particular shot, for He-like lines Ti1 and Ti1' the ratio H/V is almost equal and less than 1 (i.e. negative polarization). It indicates the energy of electron beams higher than 30 keV (see Fig. 11). More experimental data is needed to refine this technique to estimate line polarization and energy of electron beams with sufficient accuracy.

In addition to the resonance lines and satellite lines the relative intensities of the "cold" Ti K_{α} line (from wire material) and the "cold" Fe K_{α} line (from the stainless steel anode) were measured [39]. It was shown that the relative intensities of both "cold" lines have their minimum values for shot 39 when the largest polarization was observed. This means that observation of strong characteristic lines does not necessarily indicate the presence of electron beams responsible for line polarization. It would be interesting to study the polarization of the "cold" Ti K α line and its application for Z-pinch plasma diagnostics.

4. Conclusion

The development of x-ray diagnostics of Z-pinch plasmas during the last six years was reviewed. This development was focused on the M-shell emission of W and the K-shell emission of Ti. High temperature and density plasmas were produced from the variety of X-pinches on the 1 MA Zebra device at UNR. In particular, M-shell W radiation was generated by the implosions of X-pinches with tungsten wires combined with the wires from other lower-Z wire material such as Al and Mo. The M-shell emission of W ions is a very challenging topic for plasma diagnostics because of contributions from numerous ionization stages in a narrow spectral region that is impossible to resolve. LLNL EBIT data produced at various beam energies and recorded by a high-resolution crystal spectrometer and a broadband microcalorimeter allowed us to break down this very complicated M-shell spectrum into spectra with a limited number of ionization stages. LLNL EBIT data helped not only to identify the spectra from X-pinches but also to benchmark the theoretical modeling.

The results of polarization-sensitive experiments with Ti X-pinches on the Zebra at UNR were also reviewed. It was shown that the difference in polarization-dependent spectra provided information about the existence of electron beams in Z-pinch plasmas. Refinement of the technique should also provide a value of the average energy of the beams. Polarization-dependent spectra of the Ti K-shell emission generated by a quasi-Maxwellian beam at the LLNL EBIT facility were studied, and the usefulness of these data for x-ray spectropolarimetry was emphasized. Also the importance of the ability of EBIT to simulate a quasi-Maxwellian beam for benchmarking theoretical calculations was demonstrated.

Acknowledgement

This work was supported by NNSA under DOE Cooperative Agreement DE-FC52-06NA27588 and in part by DE-FC52-06NA27586 and DE-FC52-06NA27616. Work at UC, LLNL was performed under of auspices of the DOE under contract No. W-7405-Eng-48.

References

[1] P.G. Burkhalter, C.M. Dozier, D.J. Nagel. Phys. Rev. A **15**, 700 (1977).

[2] A. Zigler, H. Zmora, N. Spector et al. JOSA **70**, 129 (1980).

[3] N. Tragin, J.-P. Geindre, P. Monier et al. Phys. Scr. **37**, 72 (1988).

[4] R.B. Spielman, C. Deeney, G.A. Chandler et al. Phys. Plasmas **5**, 2105 (1998).

[5] C. Deeney, M.R. Douglas, R.B. Spielman et al. Phys. Rev. Lett. **81**,4883 (1998).

[6] M.E. Cuneo et al. Phys. Rev. Lett. **88**, 215004 (2002).

[7] M.E. Cuneo, E.M. Waisman, S.V. Lebedev et al. Phys. Rev. E **71**, 046406 (2005).

[8] V.L. Kantsyrev, A.S. Safronova, V.V. Ivanov et al. JQSRT **99**, 349 (2006).

[9] A.S. Safronova, V.L. Kantsyrev, N.D. Ouart et al. JQSRT **99**, 560 (2006).

[10] V. L. Kantsyrev, A. S. Safronova, D. A. Fedin *et al.* IEEE Trans. Plasma Sci. **34**, 194 (2006).

[11] A. Safronova, V. Kantsyrev, D. Fedin, F. Yilmaz, T. Hoppe, V. Nalajala, J. Douglass, R. McBride, M. Mitchell, L. Maxson, D. Hammer. Proc 6 th International Conf. on Dense Z-pinches, AIP CP**808**, 145 (2006).

[12] A. Safronova, V. Kantsyrev, D. Fedin, F. Yilmaz, T. Hoppe, V. Nalajala, J. Douglass, R. McBride, M. Mitchell, L. Maxson, D. Hammer. IEEE Trans. Plasma Sci. **34**, 194 (2006).

[13] T.A. Shelkovenko, D.B. Sinars, S.A. Pikuz et al. Phys. Plasmas **8**, 1305 (2001).

[14] A.S. Shlyaptseva, R.C.Mancini, P. Neill, P. Beiersdorfer. RSI **68**, 1095 (1997).

[15] A.S. Shlyaptseva, R.C.Mancini, P. Neill, P. Beiersdorfer, J.R. Crespo-López-Urrutia, K. Widmann. Phys. Rev. A **57**, 888 (1998).

[16] A.S. Shlyaptseva, R.C. Mancini, P. Neill, P. Beiersdorfer. J. Phys. B **32**, 1041 (1999).

[17] M.F. Gu. AIP Conference proceedings **730**, 127 (2004).

[18] S.M. Hamasha, A.S. Shlyaptseva, U.I. Safronova. Can. J. Phys. **82**, 331 (2004).

[19] U.I. Safronova , A.S. Safronova, S.M. Hamasha, P. Beiersdorfer. Atomic Data and Nuclear Data Tables **96**, 47 (2006).

[20] U.I. Safronova, A.S. Safronova, P. Beiersdorfer. J. Phys. B **39**, 4491 (2006).

[21] P. Neill, C. Harris, A.S. Safronova, S.M. Hamasha, S.B.Hansen, P. Beiersdorfer, U.I. Safronova. Can. J. Phys. **82**, 931 (2004).

[22] A.S. Shlyapsteva, D.A. Fedin, S.M. Hamasha, C. Harris, V.L. Kantsyrev, P. Neill, N. Ouart, U.I. Safronova, P. Beiersdorfer, K. Boyce, G.V. Brown, R. Kelley, C.A. Kilbourne, F.S. Porter, RSI **75**, 1947 (2004).

[23] F.S. Porter et al. RSI **75**, 3772 (2004).

[24] F.S. Porter et al (this journal).

[25] S.B. Hansen. PhD Dissertation, University of Nevada, Reno, 2003.

[26] S.B. Hansen and A.S. Shlyaptseva. Phys. Rev. E **70**, 036402 (2004).

[27] M. Bitter, K.W. Hill, M. Zarnstrorff et al. Phys. Rev. A **32**, 3011 (1985).

[28] P. Lee, A.J. Lieber, R.P. Chase, A.K. Pradhan. PRL **55**, 386 (1985).

[29] P. Beiersdorfer, V. Decaux, S.R. Elliott, K. Widmann, K. Wong. RSI **66**, 303 (1995).

[30] P. Beiersdorfer, G. Brown, S. Utter, P. Neill, A.J. Smith, R.S. Thoe. Phys. Rev.

A **60**, 4156 (1999).

[31] A.S. Shlyaptseva, D.A. Fedin, S.M. Hamasha, S.B. Hansen, C. Harris, V.L. Kantsyrev, P. Neill, N. Ouart, P. Beiersdorfer, U.I. Safronova. RSI **74**, 1947 (2003).

[32] D.W. Savin, P. Beiersdorfer, S.M. Kahn et al. RSI **71**, 3362 (2000).

[33] D. W. Savin et al (this journal).

[34] S.B. Hansen, A. Ya. Faenov, T.A. Pikuz, K.B. Fournier, R. Shepherd, H. Chen, K. Widmann, S.C. Wilks, Y. Ping, H.K. Chung, A. Niles, J.R. Hunter, G. Dyer, T. Ditmire. Phys. Rev. E **72,** 036408 (2005).

[35] P. Beiersdorfer, D.A. Vogel, K.J. Reed, V. Decaux, J.H. Scofield, K. Widmann, G. Hölzer, E. Förster, O. Wehrhan, D.W. Savin, L. Schweikhard. Phys. Rev. A **53**, 3974 (1996).

[36] A.S. Shlyaptseva, V.L. Kantsyrev, B.S. Bauer, P. Neill, C. Harris, D.A. Fedin, S. Hansen, N. Ouart, P. Beiersdorfer, A.G. Petrashen, U.I. Safronova. *Proceedings of the 3rd PPS Workshop*. Eds. P. Beiersdorfer and T. Fujimoto, University of California LLNL Report UCRL-ID-146907, 339 (2001).

[37] A.S. Shlyaptseva, S. Hansen, V. L. Kantsyrev, S. A. Kazantsev, A.G. Petrashen, U.I. Safronova. *Proceedings of the 3rd PPS Workshop*. Eds. P. Beiersdorfer and T. Fujimoto, University of California LLNL Report UCRL-ID-146907, 93 (2001).

[38] A.S. Shlyaptseva, V.L. Kantsyrev, N.D. Ouart, D.A. Fedin, P. Neill, C. Harris, S.M. Hamasha, S.B. Hansen, U.I.Safronova, P. Beiersdorfer, A.G. Petrashen. *Proceedings of the 4th PPS Workshop.* Eds. T. Fujimoto and P. Beiersdorfer, NIFS-PROC **57**, 47 (2004).

[39] A.S. Shlyaptseva, V.L. Kantsyrev, N. Ouart, D. Fedin, S. Hamasha, S. Hansen. *Proceedings of SPIE* **5196**, 16 (2004).

Table 1.

Wavelengths (λ in Å) a nd radiative transition rates (Ar in s^{-1}) for the strongest E1 and E2 transitions from excited states with J=1 and 2 into the ground state in Ni-like W calculated by RMBPT [18-20] and FAC [17] codes.

Line	Upper level LS	RMBT λ (Å)	RMBT Ar (s^{-1})	FAC λ (Å)	FAC Ar (s^{-1})
Ni1	3d6f $^1P_1$	3.803	5.30[13]	3.805	6.51[13]
Ni2	3d6f $^3D_1$	3.879	5.66[13]	3.880	7.25[13]
Ni3	3d5f $^1P_1$	4.308	1.16[14]	4.309	1.33[14]
NI4	3d5f $^3D_1$	4.403	9.07[13]	4.405	1.02[14]
Ni5	3p4d $^1P_1$	5.201	9.35[13]	5.195	9.54[13]
Ni6	3p4s $^1P_1$	5.689	3.72[14]	5.686	3.99[14]
Ni7	3d4f $^3D_1$	5.870	1.18[14]	5.872	1.24[14]
Ni8	3d4f $^3P_1$	6.154	2.21[13]	6.144	2.17[13]
Ni9	3d4p $^3D_1$	7.027	1.27[13]	7.028	1.21[13]
Ni10	3d4p $^3P_1$	7.174	6.67[12]	7.175	6.32[12]
Ni11	3d4s $^1D_2$	7.608	4.04[09]	7.610	4.55[09]
Ni12	3d4s $^3D_2$	7.929	5.32[09]	7.930	5.97[09]

Table 2.

K-shell Ti lin es im portant in the diagn ostics of low-den sity plasmas.

Iso- electronic sequence	Line	Transition	λ(Å)
He-like	w	1s2p $^1P_1 \rightarrow 1s^2\ ^1S_0$	2.6105
He-like	x	1s2p $^3P_2 \rightarrow 1s^2\ ^1S_0$	2.6192
He-like	y	1s2p $^3P_1 \rightarrow 1s^2\ ^1S_0$	2.6229
Li-like	q	1s2s2p $^2P_{3/2} \rightarrow 1s^22s\ ^1S_0$	2.6277
Li-like	r	1s2s2p $^2P_{1/2} \rightarrow 1s^22s\ ^1S_0$	2.6300
He-like	z	1s2s $^3S_1 \rightarrow 1s^2\ ^1S_0$	2.6370

Table 3.

Ratios of the K-shell T i line intensities from LLNL EBIT experim ents produced by a monoenergetic electron beam centered at 4.8 keV and a quasi-Maxwellian electron beam at Te=2.3 keV at LLNL EBIT.

	E_b=4800 eV monoenergetic beam [30]			T_{max}=2.3 keV quasi-Maxwellian beam [31]		
	Si(220)	Se(111)		Si(220)	Ge(111)	
	I_1	I_2	I_1/I_2	I_3	I_4	I_3/I_4
y/w	0.147	0.235	0.63	0.113	0.153	0.74
x/w	0.102	0.191	0.53	0.068	0.145	0.47
z/w	0.258	0.343	0.75	0.212	0.335	0.63
q/w	0.313	0.316	0.99	0.184	0.255	0.72

Table 4.

Comparison of polarization degrees for the K-shell Ti lines excited by monoenergetic electron beams with the energy of 4.8 and 11.5 keV.

	4.8 keV			11.5 keV
	theory[30]	exp[30]	theory	theory
w	+0.608	$+0.43^{+0.14}_{-0.12}$	+0.607	+0.481
y	-0.339	$-0.33^{+0.07}_{-0.07}$	-0.309	+0.228
x	-0.519	$-0.48+^{0.06}_{-0.06}$	-0.513	-0.418
z	-0.106	$-0.101^{+0.014}_{-0.013}$	-0.106	-0.096
q	+0.341	$+0.40^{+0.15}_{-0.1}$	+0.340	+0.270

Table 5.

Measured values of the intensities of lines recorded by a horizontal (H) and a vertical (V) spectrometers in Ti X-pinch experiments.

Iso-elect. seq.	Line	Shot 36			Shot 37			Shot 39		
		H	V	H/V	H	V	H/V	H	V	H/V
He-like	Ti1(w)	2.19[7]	1.90[7]	1.15	2.79[7]	2.68[7]	1.04	2.97[7]	3.66[7]	0.81
He-like	Ti1′(y)	1.98[7]	1.58[7]	1.25	2.38[7]	2.08[7]	1.14	2.62[7]	3.21[7]	0.82
Li-like	Ti1′′(q)	1.69[7]	1.30[7]	1.30	1.79[7]	1.54[7]	1.16	2.36[7]	2.20[7]	1.07
Be-like	Ti1′′′	6.48[6]	5.23[6]	1.24	6.47[6]	5.22[6]	1.24	9.81[6]	7.34[6]	1.34
Low ion.	Ti4(K_α)	2.30[7]	2.24[7]	1.03	1.90[7]	1.64[7]	1.16	1.64[7]	1.43[7]	1.15

Figure Captions

Fig. 1. Experimental M-shell spectrum of W ions from the LLNL EBIT-II facility recorded by a crystal spectrometer at E_b=3.6 keV (bottom) and theoretical synthetic spectrum calculated for a Gaussian electron distribution function of FWHM=50 eV centered at 3.6 keV (top). Intense spectral features are identified by the iso-electronic sequence.

Fig. 2. Experimental M-shell spectrum of W ions from the LLNL EBIT-II facility recorded by a crystal spectrometer at E_b=3.9 keV (bottom) and theoretical synthetic spectrum calculated for a Gaussian electron distribution function of FWHM=50 eV centered at 3.9 keV (top). Intense spectral features are identified by the iso-electronic sequence.

Fig. 3. Experimental M-shell spectrum of W ions from the LLNL EBIT-II facility recorded by a crystal spectrometer at E_b=4.3 keV (bottom) and theoretical synthetic spectrum calculated for a Gaussian electron distribution function of FWHM=50 eV centered at 4.3 keV (top). Intense spectral features are identified by the iso-electronic sequence.

Fig. 4. The fourteen M-shell spectra of W ions from LLNL EBIT-I device recorded by the 14 pixels of the XRS microcalorimeter at E_b=3.9 keV.

Fig. 5. Experimental M-shell spectrum of W ions from the LLNL EBIT-I device recorded by the XRS microcalorimeter at E_b=3.9 keV (bottom) and theoretical synthetic spectrum calculated for a Gaussian electron distribution function of FWHM=50 eV centered at 3.9 keV (top). Intense spectral features are identified by

the iso-electronic sequence.

Fig. 6. Experimental spectrum from the Zebra Al/W X-pinch (top) and experimental M-shell spectrum of W ions from the LLNL EBIT-I electron ion beam trap recorded by the XRS microcalorimeter at E_b=3.9 keV (bottom).

Fig. 7. Experimental spectrum from the Zebra W/Mo X-pinch (top) and experimental M-shell spectrum of W ions from the LLNL EBIT-I electron ion beam trap recorded by the XRS microcalorimeter at E_b=3.9 keV (bottom).

Fig. 8. Experimental combined Al/W (black) and W/Mo (grey) X-pinch spectra fit with a synthetic spectrum from our model at Te=1 keV, Ne=10^{21} cm^{-3}, and f=0.03 (light grey).

Fig. 9. Theoretical synthetic spectra of K-shell Ti calculated at low density for two different electron distribution functions: a Gaussian of FWHM=50 eV centered at 4.8 keV (grey line) and a Maxwellian at T_M=2.3 keV (black line).

Fig. 10. Theoretical synthetic spectra of K-shell Ti calculated at Te=1 keV and Ne=10^{21} cm^{-3} (a) and at Te=2.2 keV and Ne=10^{22} cm^{-3} (b) are used for the interpretation of the typical Ti X-pinch spectrum (c).

Fig. 11. Polarization of the most intense K-shell Ti lines as a function of the electron beam energy. Identification of these lines is given in Table 2.

Fig. 12. Comparison of experimental (grey line) and theoretical (black line) dielectronic recombination spectra of K-shell Ti. The experimental spectrum was produced on LLNL EBIT recorded with a von Hámos type crystal spectrometer employing a Si (220) crystal.

Fig. 13. Polarization-sensitive K-shell spectra from a Ti X-pinch produced at the 1 MA Zebra facility at UNR. The spectra were simultaneously recorded by the horizontal (top) and vertical (bottom) spectrometers (Zebra shot 39).

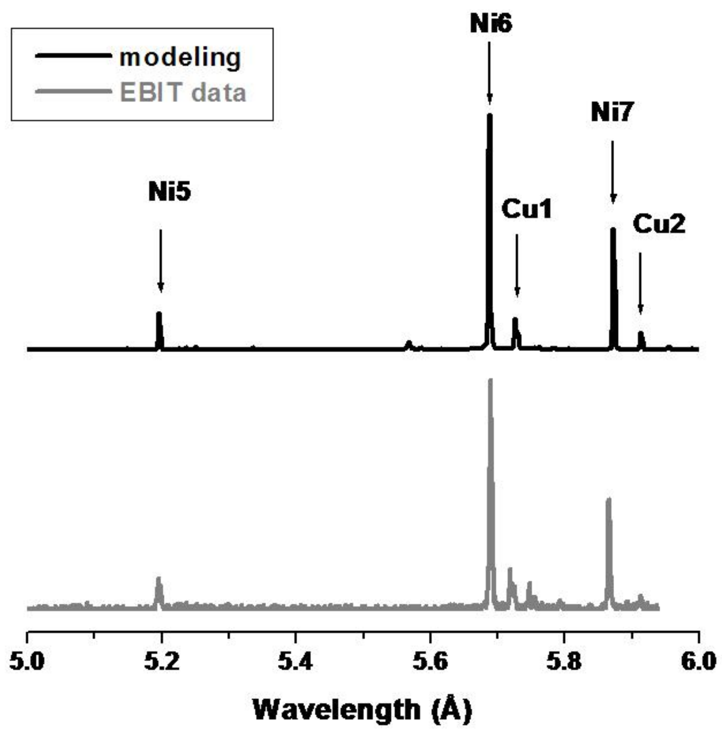
modeling
EBIT data
Ni6
Ni7
Ni5
Cu1
Cu2
5.0
5.2
5.4
5.6
5.8
6.0
Wavelength (Å)

Fig. 1.

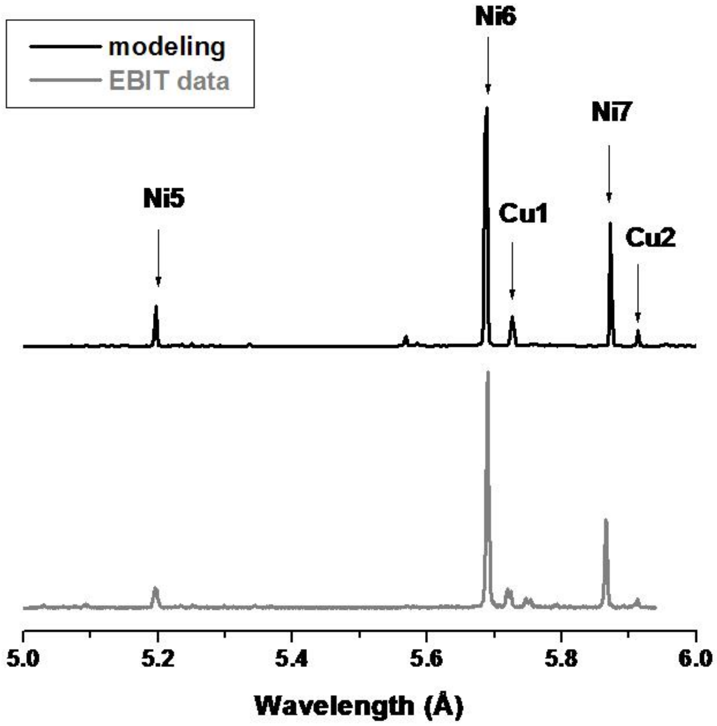
modeling
EBIT data
Ni6
Ni7
Ni5
Cu1
Cu2
5.0
5.2
5.4
5.6
5.8
6.0
Wavelength (Å)

Fig. 2.

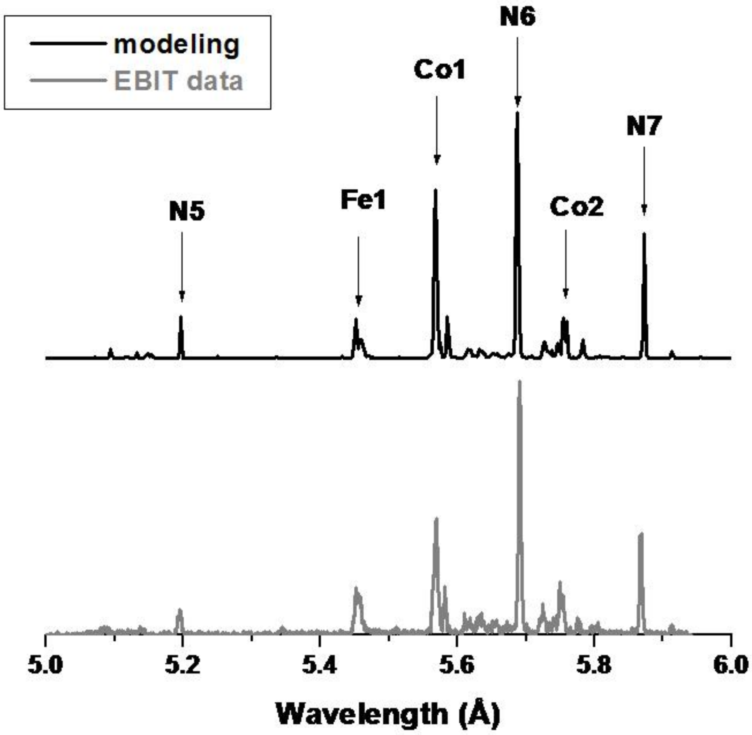
modeling
EBIT data
N6
Co1
N7
N5
Fe1
Co2
5.0
5.2
5.4
5.6
5.8
6.0
Wavelength (Å)

Fig. 3.

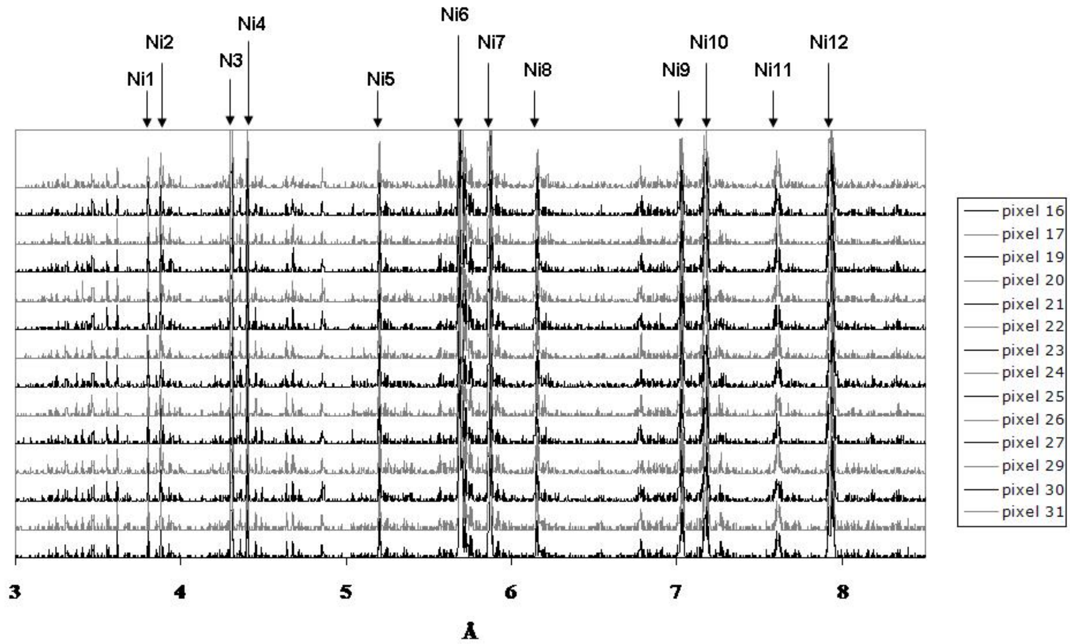
Ni1
Ni2
N3
Ni4
Ni5
Ni6
Ni7
Ni8
Ni9
Ni10
Ni11
Ni12
pixel 16
pixel 17
pixel 19
pixel 20
pixel 21
pixel 22
pixel 23
pixel 24
pixel 25
pixel 26
pixel 27
pixel 29
pixel 30
pixel 31
3
4
5
6
7
8
Å

Fig. 4.

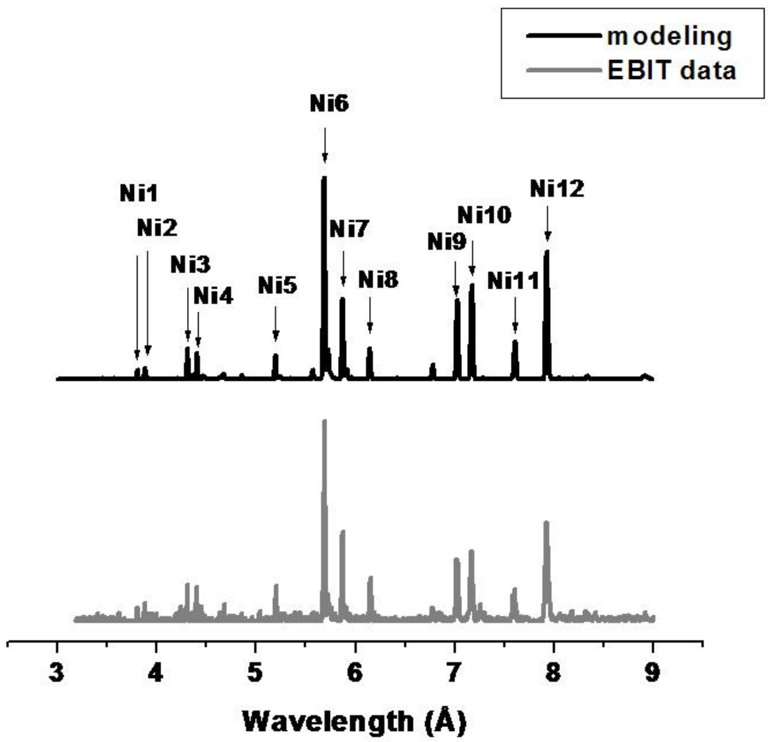
modeling
EBIT data
Ni1
Ni2
Ni3
Ni4
Ni5
Ni6
Ni7
Ni8
Ni9
Ni10
Ni11
Ni12
3
4
5
6
7
8
9
Wavelength (Å)

Fig. 5.

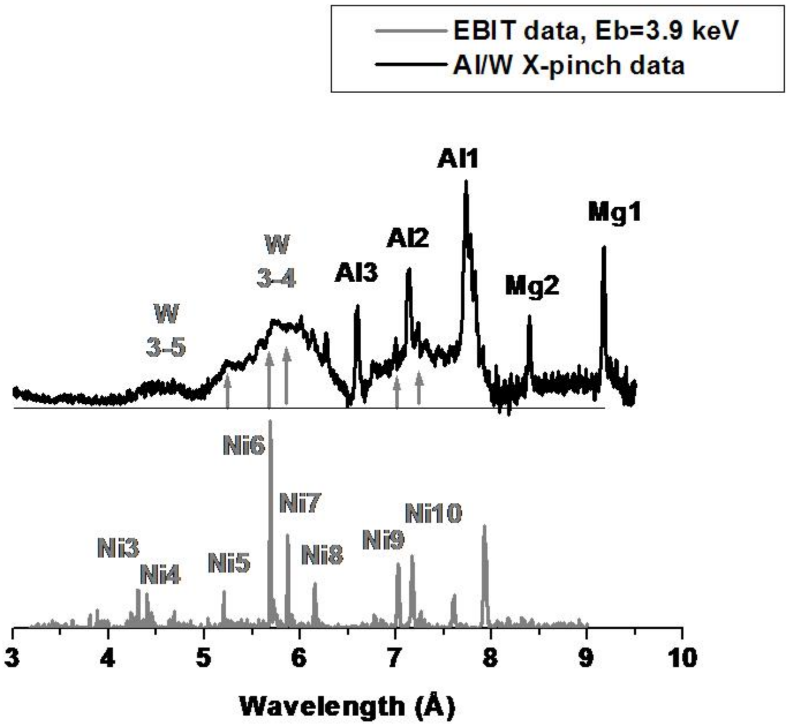
EBIT data, Eb=3.9 keV
Al/W X-pinch data
Al1
Al2
Al3
Mg1
Mg2
W
3-4
W
3-5
Ni3
Ni4
Ni5
Ni6
Ni7
Ni8
Ni9
Ni10
3
4
5
6
7
8
9
10
Wavelength (Å)

Fig. 6.

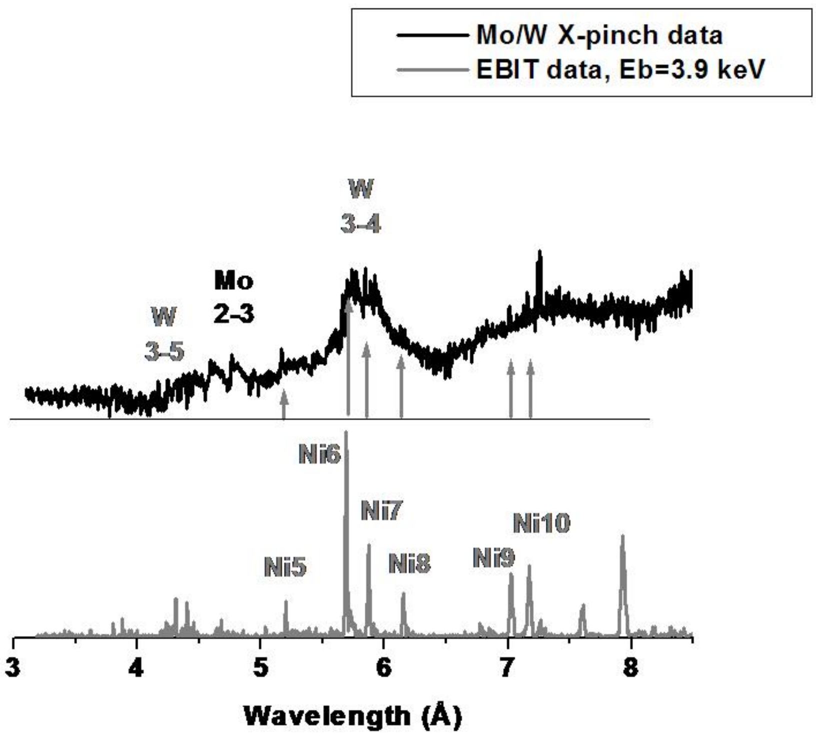
Mo/W X-pinch data
EBIT data, Eb=3.9 keV
W
3-4
Mo
2-3
W
3-5
Ni6
Ni7
Ni10
Ni5
Ni8
Ni9
3
4
5
6
7
8
Wavelength (Å)

Fig. 7.

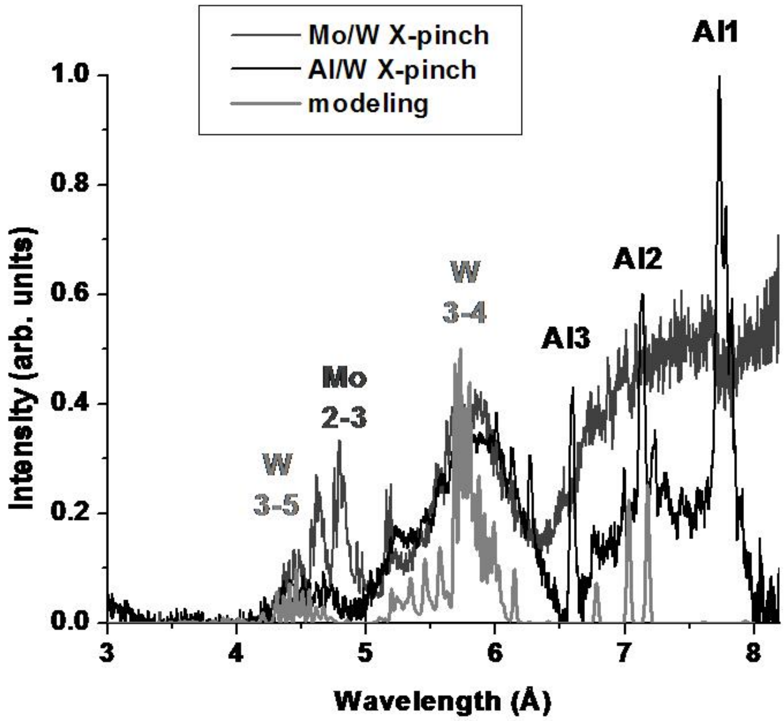
Mo/W X-pinch
Al/W X-pinch
modeling
Al1
Al2
Al3
W
3-4
Mo
2-3
W
3-5
Intensity (arb. units)
Wavelength (Å)
1.0
0.8
0.6
0.4
0.2
0.0
3
4
5
6
7
8

Fig. 8.

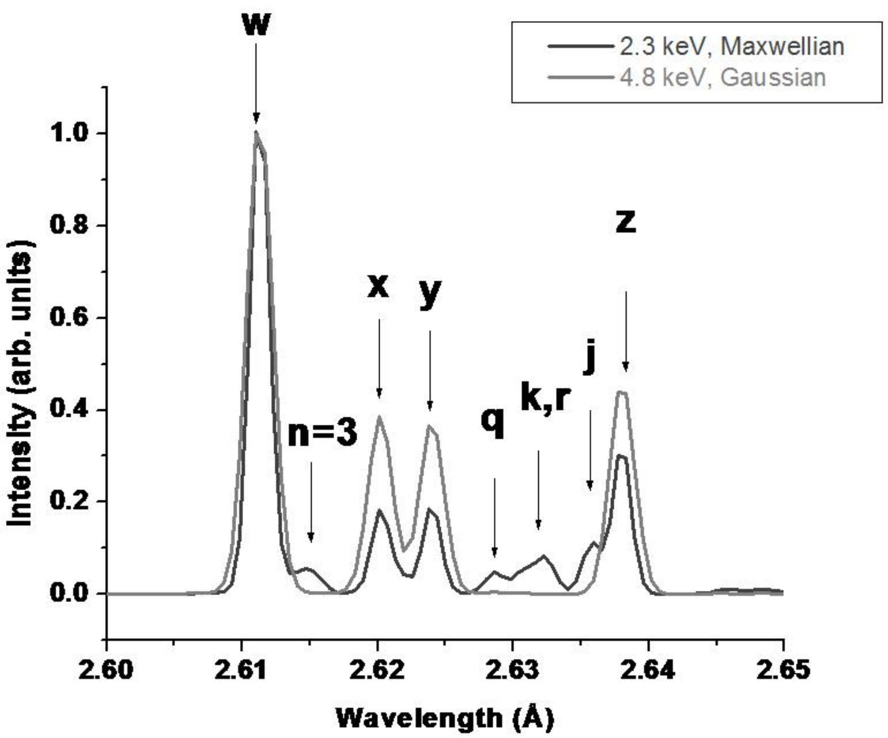
w
2.3 keV, Maxwellian
4.8 keV, Gaussian
1.0
0.8
0.6
0.4
0.2
0.0
Intensity (arb. units)
z
x
y
j
k,r
q
n=3
2.60
2.61
2.62
2.63
2.64
2.65
Wavelength (Å)

Fig. 9.

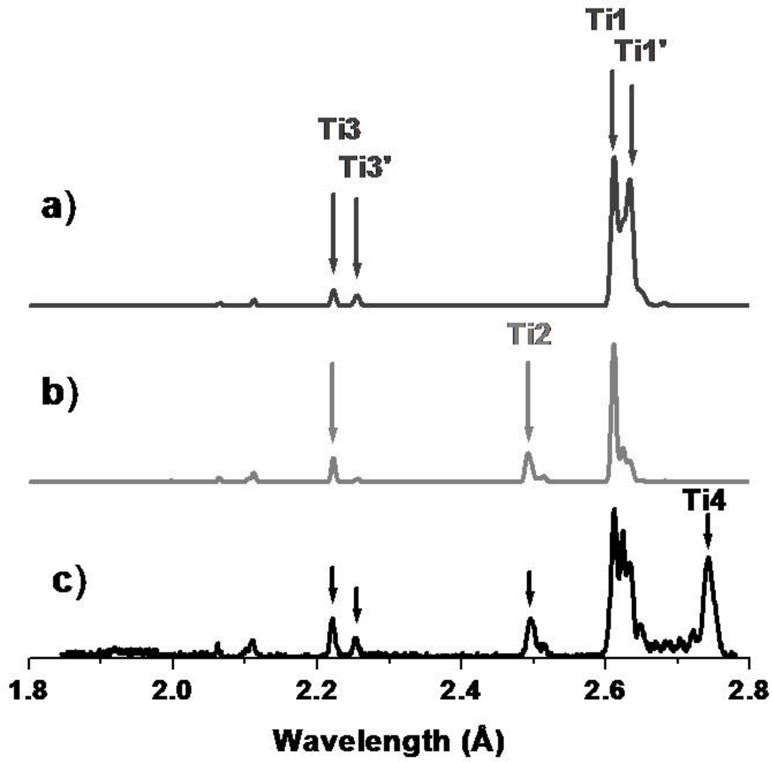

Fig. 10.

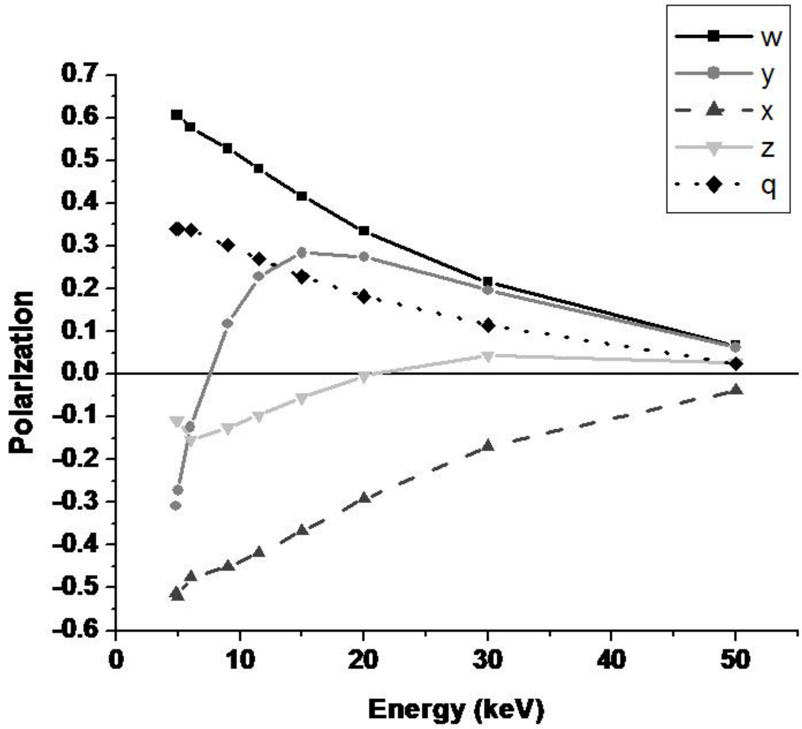
w
y
x
z
q
Polarization
0.7
0.6
0.5
0.4
0.3
0.2
0.1
0.0
-0.1
-0.2
-0.3
-0.4
-0.5
-0.6
0
10
20
30
40
50
Energy (keV)

Fig. 11.

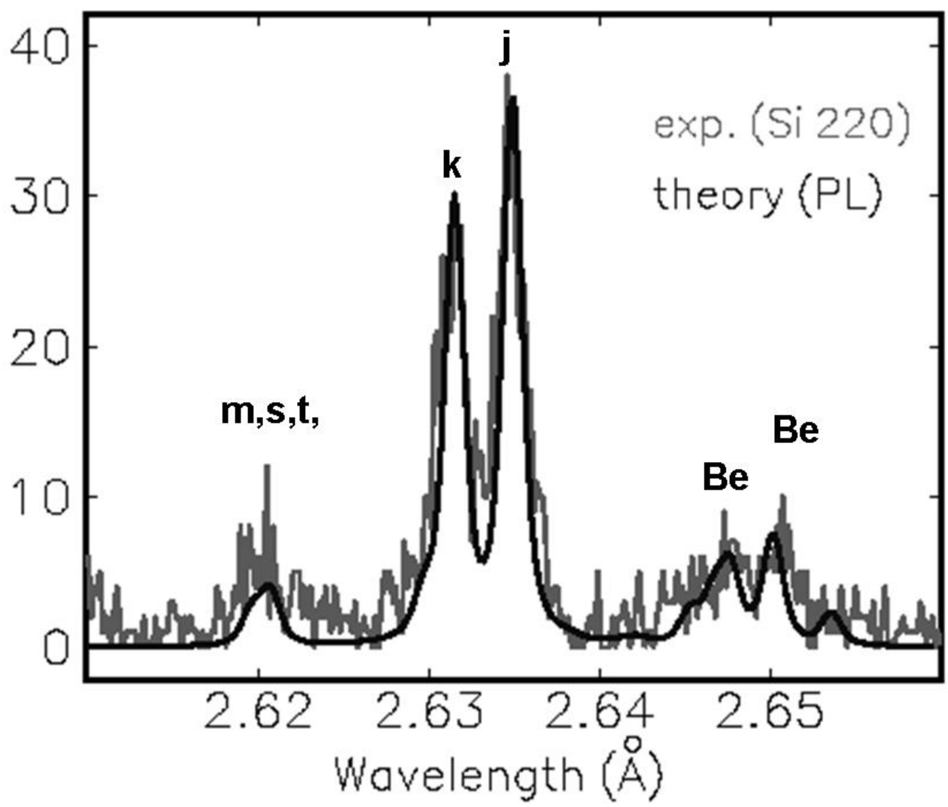
40
30
20
10
0
j
k
exp. (Si 220)
theory (PL)
m,s,t,
Be
Be
2.62
2.63
2.64
2.65
Wavelength (Å)

Fig. 12.

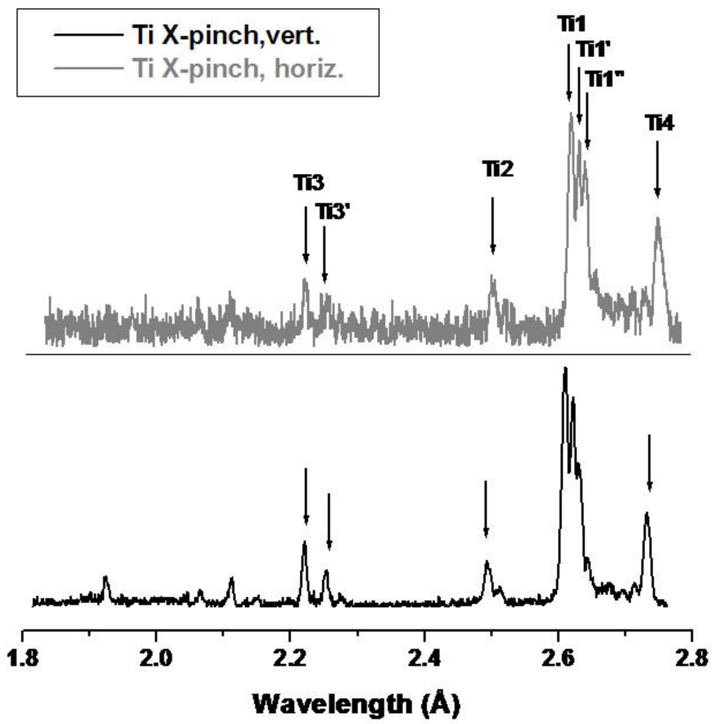
Ti X-pinch,vert.
Ti X-pinch, horiz.
Ti1
Ti1'
Ti1"
Ti4
Ti2
Ti3
Ti3'
1.8
2.0
2.2
2.4
2.6
2.8
Wavelength (Å)

Fig. 13.